nature cell biology

Selective autophagy degrades DICER and AGO2 and regulates miRNA activity

Derrick Gibbings[1,2,9], Serge Mostowy[3,4,5,6,9], Florence Jay[1], Yannick Schwab[7], Pascale Cossart[3,4,5] and Olivier Voinnet[1,8,10]

MicroRNAs (miRNAs) form a class of short RNAs (~21 nucleotides) that post-transcriptionally regulate partially complementary messenger RNAs. Each miRNA may target tens to hundreds of transcripts to control key biological processes. Although the biochemical reactions underpinning miRNA biogenesis and activity are relatively well defined[1,2] and the importance of their homeostasis is increasingly evident, the processes underlying regulation of the miRNA pathway *in vivo* are still largely elusive[3]. Autophagy, a degradative process in which cytoplasmic material is targeted into double-membrane vacuoles, is recognized to critically contribute to cellular homeostasis. Here, we show that the miRNA-processing enzyme, DICER (also known as DICER1), and the main miRNA effector, AGO2 (also known as eukaryotic translation initiation factor 2C, 2 (EIF2C2)), are targeted for degradation as miRNA-free entities by the selective autophagy receptor NDP52 (also known as calcium binding and coiled-coil domain 2 (CALCOCO2)). Autophagy establishes a checkpoint required for continued loading of miRNA into AGO2; accordingly, NDP52 and autophagy are required for homeostasis and activity of the tested miRNAs. Autophagy also engages post-transcriptional regulation of the *DICER* mRNA, underscoring the importance of fine-tuned regulation of the miRNA pathway. These findings have implications for human diseases linked to misregulated autophagy, DICER- and miRNA-levels, including cancer.

Following their export to the cytoplasm, stem-loop precursor (pre)-miRNAs are cleaved by Dicer into ~21-base-pair double-stranded miRNA–miRNA* duplexes and transferred into the groove of argonaute proteins (AGO). On miRNA*-strand dissociation, a mature single-stranded miRNA remains loaded into, and stabilized by, AGO (ref. 1). AGO then detaches from DICER to bind TNRC6 (ref. 4), an essential cofactor in the miRNA-induced silencing complex (miRISC). Activated miRISC can then repress miRNA-targeted mRNA by inhibiting its translation and accelerating its decay[2,5]. The mechanisms regulating RNA and protein components of miRNA pathways *in vivo* have only recently gained attention in mammals. Hence, mammalian miRNA turnover can be enhanced through nucleotide trimming–tailing[6] or the exonuclease Xrn2 (ref. 7), and limited evidence suggests that a fraction of unloaded Ago may be selectively targeted for degradation[8]. Interestingly, DICER protein levels undergo fine-tuning mediated both by DICER substrates through competition of pre-miRNA with *DICER* mRNA for XPO5-dependent nuclear-cytoplasmic export, and by DICER products through repression of the *DICER* mRNA by specific mature miRNAs in distant organisms including humans[9] and plants[10]. Thus, a requirement for fine-tuned, homeostatic regulation of miRNA pathways seems to be conserved across kingdoms.

Macroautophagy (herein referred to as autophagy) is an intracellular degradation process contributing to cellular homeostasis[11]. Thirty-six conserved autophagy-related (ATG) proteins control the initiation and elongation of double-membrane autophagosomes, engulfing cargoes that are ultimately degraded on fusion with lysosomes[11]. Selective degradation is enabled by autophagy receptors, including p62 (SQSTM1; ref. 12) and NDP52 (ref. 13), that bind both cytosolic substrates and Atg8 (that is, LC3) family proteins inserted into the autophagosome membrane. The detailed molecular mechanisms underpinning cargo selectivity are only emerging. Accordingly, autophagy receptors may confer some cargo selectivity by recognizing conjugated ubiquitin[14], although this may also occur through recognition of other modifications or molecules independently of ubiquitin[13,15]. It has previously been shown that several miRNA

[1]Swiss Federal Institute of Technology (ETH-Z), Department of Biology, Zürich 8092, Switzerland. [2]University of Ottawa, Department of Cellular and Molecular Medicine, Ottawa K1H 8M5, Canada. [3]Institut Pasteur, Unité des Interactions Bactéries-Cellules, Département de Biologie Cellulaire et Infection, 75015 Paris, France. [4]Inserm, Unité 604, 75015 Paris, France. [5]INRA, USC2020, 75015 Paris, France. [6]Section of Microbiology, MRC Centre for Molecular Bacteriology and Infection, Imperial College London, Armstrong Road, London SW7 2AZ, UK. [7]Institut de Génétique et de Biologie Moléculaire et Cellulaire, Centre National de la Recherche Scientifique, Unité Mixte de Recherche 7104, Institut National de la Santé et de la Recherche Médicale Unité 964, 1 rue Laurent Fries, 67404 Illkirch, France. [8]Institut de Biologie Moléculaire des Plantes (IBMP), 12 rue du Général Zimmer, 67084 Strasbourg Cedex, France. [9]These authors contributed equally to this work. [10]Correspondence should be addressed to O.V. (e-mail: voinneto@ethz.ch)

Received 7 September 2012; accepted 2 October 2012; published online 11 November 2012; DOI: 10.1038/ncb2611

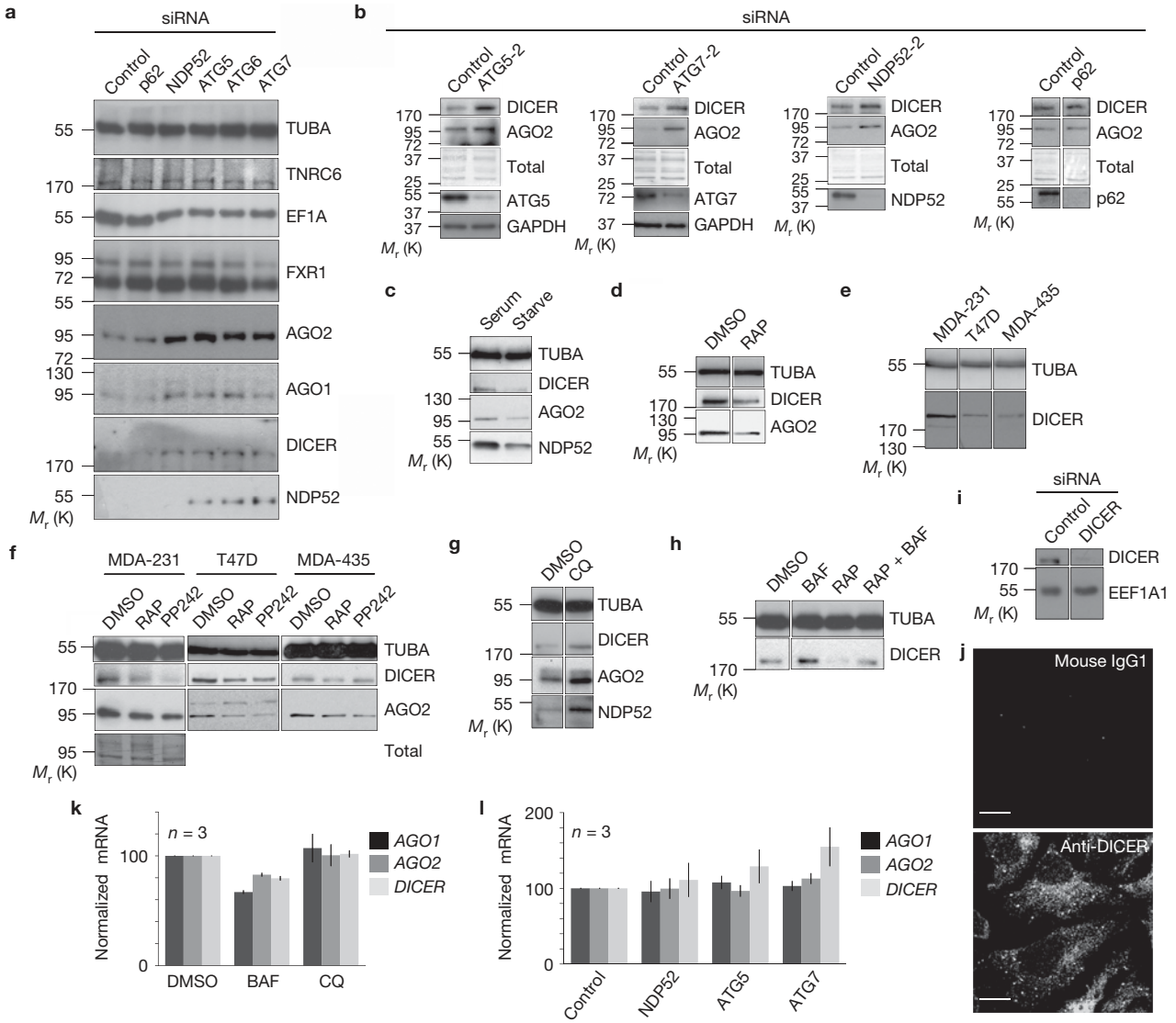

Figure 1 Levels of DICER and AGO proteins are regulated by autophagy. (**a**) Western blot analysis of HeLa cells treated with siRNA for 84 h. (**b**) Western blot analysis of HeLa cells treated with a second independent siRNA targeting ATG5, ATG7 or NDP52. GAPDH and total protein stained with Coomassie blue serve as loading controls. (**c**) Western blot analysis of HeLa cells cultured in Hank's buffered salt solution (Starved) or DMEM+ 10% FBS (Serum). (**d**) Western blot analysis of HeLa cells treated (48 h) with an inhibitor of mTORC1 (RAP, 20 nM) or control (DMSO). (**e**) Western blot analysis comparing the levels of DICER in MDA-231, T47D and MDA-435 cells. (**f**) Western blot analysis of MDA-231, T47D and MDA-435 cells treated (48 h) with inhibitors of mTORC1 (RAP, 20 nM), mTORC1 and 2 (PP242, 100 nM), or DMSO (control). (**g**) Western blot analysis of HeLa cells treated with CQ or DMSO for 12 h. (**h**) Western blot analysis of HeLa cells treated with BAF (200 nM, 12 h), RAP (20 nM, 24 h), or RAP and BAF. The results in **a**–**h** are representative of three experiments and use α-tubulin (TUBA) as a loading control. (**i**) Western blot analysis of DICER (monoclonal antibody 13D6) or control (EEF1A1) in HeLa cells treated with control siRNA or siRNA targeting DICER. (**j**) Confocal analysis of the signal from an anti-DICER monoclonal antibody (clone 13D6) or an isotype control monoclonal antibody in HeLa cells. Scale bar, 10 μm. (**k**,**l**) RT–qPCR analysis of *AGO1*, *AGO2* and *DICER* mRNA in HeLa cells treated for 12 h with DMSO, BAF or CQ (**k**) or siRNA for 84 h (**l**). Error bars show s.e.m. Uncropped images of blots are shown in Supplementary Fig. S3.

pathway components, including DICER, AGO and TNRC6, associate with membranes[16–18]. In this context, we proposed that autophagy might modulate the levels of these or other proteins or RNAs involved in miRNA biogenesis and action, by promoting their regulated degradation[19].

To investigate the potential contribution of autophagy to the degradation of cytosolic miRNA-containing complexes, HeLa cells were depleted of the key autophagy components ATG5, ATG6 or ATG7, or of the selective autophagy receptors NDP52 or p62 using short interfering RNAs (siRNAs). AGO2, AGO1 and DICER accumulated in cells depleted of ATG5, ATG6, ATG7 or NDP52, but not of p62 (Fig. 1a,b). In contrast, siRNA-mediated depletion of the autophagy machinery did not result in elevated levels of the key miRISC component TNRC6 (ref. 4), the AGO-interacting protein FXR1 or EF1A, an AGO-binding protein that mediates AGO-dependent inhibition of translational elongation[20] (Fig. 1a). Activating autophagy by serum starvation or with an mTOR inhibitor (rapamycin, (RAP)) decreased DICER and AGO2 levels (Fig. 1c,d). DICER levels vary among representative cell lines (Fig. 1e), and DICER levels decreased in each line tested on treatment with mTOR inhibitors (RAP, PP242; Fig. 1f). Conversely,

DICER and AGO2 levels increased in HeLa cells treated with inhibitors of lysosomal acidification (bafilomycin A1 (BAF), chloroquine (CQ)), known to block autophagy (Fig. 1g,h). Moreover, DICER levels decreased by RAP treatment were rescued by co-treatment with BAF (Fig. 1h). The protein detected with anti-DICER monoclonal antibody was confirmed to be DICER by its selective depletion with siRNA targeting *DICER* mRNA and specific labelling of HeLa cells by confocal microscopy, which was consistent with the uneven cytoplasmic distribution of endogenous DICER previously reported[21] (Fig. 1i,j). The effects of autophagy-modulating treatments on DICER, AGO1 and AGO2 were at the protein level, as their mRNA levels remained unchanged (Fig. 1k,l).

Analysis by confocal microscopy showed that DICER significantly co-localized with a fraction of the autophagy receptor NDP52 in HeLa cells (using Costes', Fay's or van Steensel's tests for non-random co-localization, $P < 0.0001$); moreover, this co-localization increased 3.2-fold in cells treated with RAP (Fig. 2a,b, Costes', Fay's and van Steensel's tests, $P < 0.0001$), consistent with targeting of DICER to NDP52-dependent autophagy (Fig. 1a,b). Also consistent with targeting of DICER for autophagic degradation, DICER co-localized significantly with the autophagolysosome marker HcRed–LC3 and this co-localization increased 6.7-fold in cells treated with BAF (Fig. 2c,d, Costes', Fay's or van Steensel's test, $P < 0.0001$, BAF and control treated). In contrast, no co-localization was observed between autophagy markers and GFP-labelled DCP1A, an AGO-associated mRNA decapping factor that localizes to cytoplasmic bodies[22] (P-bodies; Fig. 2e).

We then sought evidence for the physical association of DICER and AGO2 with autophagosomes. First, using electron microscopy in CQ-treated cells, we confirmed the accumulation of membrane-bound structures containing irregular electron-dense, vesicular and organellar content, hallmark features of autophagolysosomes[23], in which DICER was enriched when compared with the surrounding cytoplasm (Fig. 2f–i). Second, we isolated autophagosome- and autophagolysosome-enriched cell fractions using density gradients[24]. As expected, ubiquitin and the autophagy receptors NDP52 and p62 accumulated in fractions containing autophagosomes and autophagolysosomes in CQ-treated cells (Fig. 2j,k). In contrast, ALIX, a marker of multivesicular bodies that associate with TNRC6 (ref. 16), did not accumulate in these fractions, nor did the miRISC component TNRC6 or the P-body-associated DCP1A (Fig. 2j). In contrast, DICER and AGO2 were detected in autophagosome and autophagolysosome fractions from CQ-treated cells (Fig. 2j). Taken together, the data presented in Figs 1 and 2 strongly support the idea that autophagy degrades DICER and AGO2 in an NDP52-selective manner. These results further suggest that autophagy-mediated regulation occurs upstream of the formation of miRISC (probed with TNRC6) and miRISC activity (probed with EF1A and DCP1a).

DICER and AGO2 localize to NDP52-labelled autophagosomes (Fig. 2a,b,j) and are subject to NDP52-dependent autophagy (Fig. 1a,b), suggesting that they may interact with NDP52. Previous studies showed that NDP52 binds GEMIN4 (ref. 25), a component of the multi-protein SMN (survival of motor neuron) complex involved in mRNA splicing, which also localizes to the cytoplasm. GEMIN4 and GEMIN3 are routinely found associated with AGO proteins, in complexes also containing DICER (ref. 26), albeit for reasons not yet understood. We thus considered the possibility that GEMIN4 may link AGO2 and DICER to NDP52 and promote their autophagic degradation. GEMIN4 was detected in autophagosome-enriched fractions of CQ-treated cells and GEMIN4 levels were sensitive to depletion of ATG5, ATG6 or ATG7, and to modulation of autophagy by serum starvation or with drugs (Fig. 3a–c), suggesting that GEMIN4, similarly to DICER or AGO2, is degraded by autophagy. We confirmed that GEMIN4 immunoprecipitates with NDP52 but not with the distinct autophagy receptor, p62 (Fig. 3d). In agreement with the previously reported co-enrichment of DICER and GEMIN4 in AGO complexes[26], DICER immunoprecipitates contained GEMIN4 (Fig. 3e) and, conversely, AGO2 immunoprecipitates contained GEMIN4 and DICER (Fig. 3f). Furthermore, NDP52 co-immunoprecipitated with DICER (Fig. 3e). Collectively, these data suggest that DICER, AGO2 and GEMIN4 are targeted to autophagic degradation through their association with NDP52.

As both GEMIN3 and -4 associate with AGO (refs 26,27), the two proteins were co-depleted in subsequent investigations to prevent potential functional redundancy (Fig. 3g). AGO2 accumulated in HeLa cells depleted of GEMINs (Fig. 3h) but did not accumulate significantly further in cells depleted of both GEMINs and ATG5 (Fig. 3h), suggesting that GEMINs operate in the same pathway as ATG5, which mediates autophagy-dependent AGO2 degradation. NDP52 recognizes both ubiquitylated and ubiquitin-independent cargoes for delivery to autophagosomes[13]. In cells depleted of NDP52 or ATG5, ubiquitylated AGO2 or a ubiquitylated protein tightly associated to AGO2, accumulated to high levels (Fig. 3i). Thus, NDP52 may selectively direct AGO2 to autophagy using non-mutually exclusive and parallel recognition events including binding of AGO2 by GEMIN4 and post-translational modification of AGO2 or associated partner(s) by ubiquitin. In contrast, DICER levels were not significantly affected by depletion of GEMINs (Fig. 3h), even though DICER associates with GEMIN4 and NDP52 (Fig. 3e), co-localizes with NDP52 (Fig. 2a) and is degraded in an NDP52-dependent manner (Fig. 1b). Dicer may thus be recruited to NDP52-dependent autophagic degradation through multiple recognition events potentially compensating for the absence of GEMINs.

As lysosomes contain RNA-degrading nucleases, we investigated whether autophagy might degrade pre-miRNA or miRNA cargoes along with DICER or AGO2. The levels of ubiquituous miRNAs (for example, miR-16 and let-7a) and their corresponding miRNA* and pre-miRNA were, however, unperturbed in cells treated with BAF or ATG5-targeting siRNAs (24 h, Fig. 3j and Supplementary Fig. S1a). Similarly, mTOR inhibitors RAP or PP242 did not affect the levels of tested miRNAs (Supplementary Fig. S1b). DICER and AGO2 levels were clearly altered by these treatments (Figs 1c,h and 3j), strongly suggesting that pre-miRNA, miRNA* and miRNA are not degraded by autophagy in association with DICER or AGO2. This suggests that miRNA-free (that is, unloaded) AGO2 should specifically accumulate in autophagy-compromised cells. Indeed, significantly less miR-16 and let-7a was detected in AGO2 immunoprecipitates from BAF-treated cells (Fig. 3k). Taken together, these data suggest that a complex of DICER and AGO unattached to miRNA-related cargoes is selectively targeted for autophagy.

miRNA levels are not affected by short-term alterations to autophagy (Supplementary Fig. S1a–b), consistent with their avoidance of direct

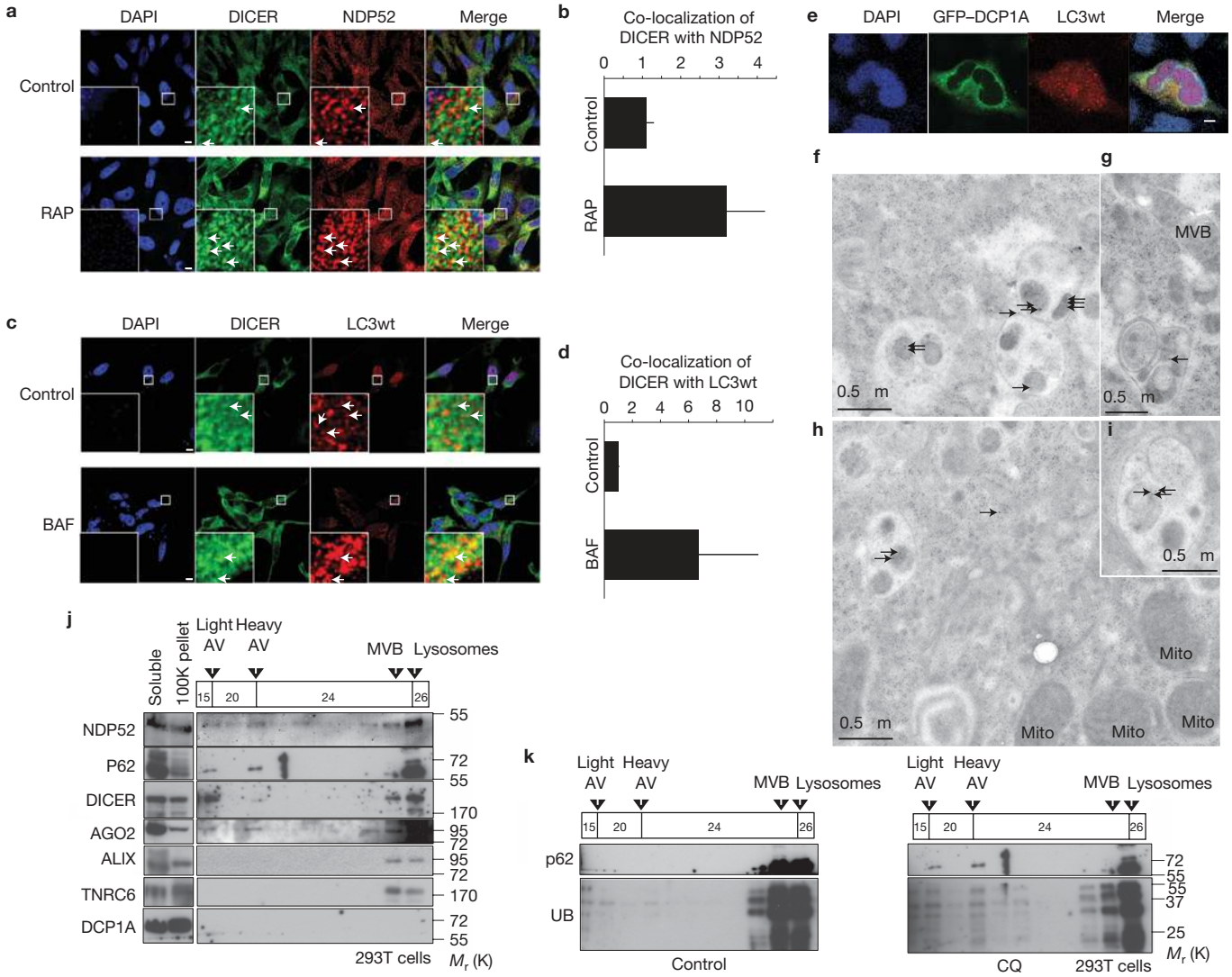

Figure 2 DICER co-localizes and associates with autophagosomes. (**a**) Localization using confocal microscopy of endogenous DICER (monoclonal antibody 13D6) and NDP52 in HeLa cells treated with RAP or control. The arrows highlight some examples of co-localization. The lower left insets show higher magnifications of the areas outlined in the main panel. Scale bars, 5 μm. (**b**) Quantification of DICER co-localization with NDP52. Total fluorescence intensity of DICER co-localized with punctae (>0.2 μm^3) of NDP52 was quantified with Volocity software in RAP-treated cells/control-treated cells over several *Z*-stacked microscope fields per experiment ($n = 4$, error bars s.e.m.). (**c**) Localization using confocal microscopy of endogenous DICER (monoclonal antibody 13D6) and HcRed–LC3 in HeLa cells treated with BAF or control. The arrows highlight some examples of co-localization. Insets as in **a**. Scale bar, 5 μm. (**d**) Quantification of DICER co-localization with HcRed–LC3 was performed as for NDP52 in **b**. (**e**) Confocal microscopy analysis of GFP–DCP1A and HcRed–LC3wt in HeLa cells. Scale bar, 10 μm. (**f–i**) Localization of DICER (monoclonal antibody 13D6) detected with anti-mouse IgG (10 nm gold beads) by electron microscopy in CQ- (20 μM, 12 h) treated HeLa cells. Mito, mitochondria; MVB, multivesicular body. The black arrows highlight all gold beads. (**j**) Western blot analysis of fractions from a discontinuous gradient of Histodenz (15%, 20%, 24%, 26%) described to enrich autophagosomes (light AV) and autophagolysosomes (heavy AV; ref. 24). HEK293T cells were treated with CQ (20 μM, 16 h). Fractions enriched in multivesicular body and lysosomal markers are indicated. Material that was pelleted by centrifugation at 100,000*g* (100 K pellet) or that remained in solution after the 100,000*g* spin (soluble) was not added to the gradient. (**k**) Western blot analysis of UB and p62 in discontinuous Histodenz gradients (as in **j**) of HEK293T cells treated with control (DMSO) or CQ. Uncropped images of blots are shown in Supplementary Fig. S3.

autophagic degradation. However, miRNAs have surprisingly long half-lives (~5 days; ref. 28), suggesting that more extended periods might be required to destabilize miRNA levels as a consequence of perturbed homeostasis of key proteins involved in their biogenesis or stability, including DICER or AGO. Levels of miR-16 and let-7a, measured by northern blotting or quantitative PCR with reverse transcription (RT–qPCR), indeed decreased significantly in cells treated with siRNAs targeting NDP52, ATG5 or ATG7, but not p62, for an extended period of 4 days (Fig. 4a,b). In contrast, pre-miR-16 and pre-let-7a levels were not overtly modified (Fig. 4a–c), suggesting that prolonged defects in autophagy specifically affect miRNA stability after pre-miRNA processing, but before miRISC formation and activity (Figs 1 and 2).

We considered the possibility that the miRNA-degrading exonuclease XRN2 might be degraded by autophagy; its excess triggered by autophagy inhibition could then cause miRNA levels to decrease. Arguing against this, XRN2 was not detectable in autophagosome-enriched

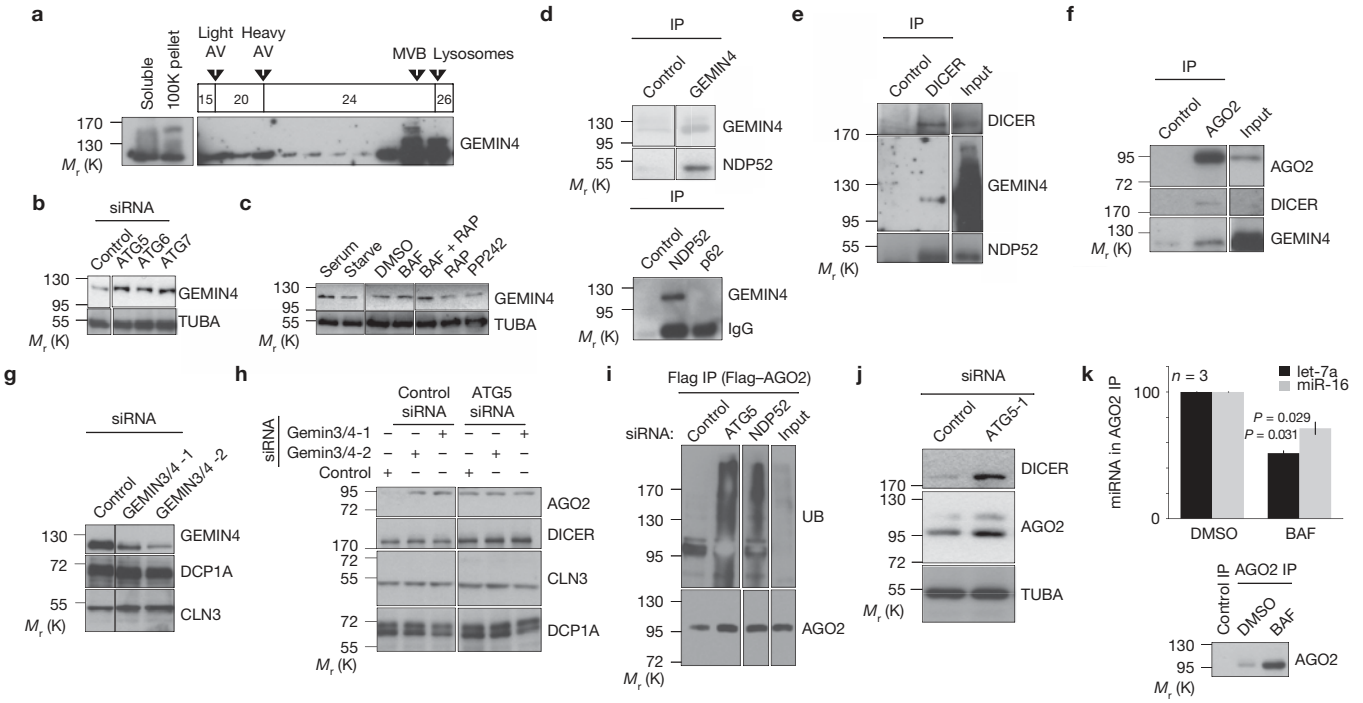

Figure 3 DICER associates with NDP52 and is targeted to autophagy independently of an RNA cargo. (**a**) Western blot analysis of GEMIN4 in fractions from a discontinuous gradient of Histodenz (15%, 20%, 24%, 26%) described to enrich autophagosomes (light AV) and autophagolysosomes (heavy AV). HEK293T cells were treated with CQ (20 μM, 16 h). Fractions enriched in multivesicular body (MVB) and lysosomal markers are indicated. (**b**) Western blot of GEMIN4 or loading control (TUBA) in HeLa cells treated with control siRNA or siRNA targeting ATG5, ATG6 or ATG7. (**c**) Western blot analysis of GEMIN4 or control (TUBA) in HeLa cells cultured in DMEM 10% FBS (Serum), Hank's buffered salt solution (Starve) for 2 h, or treated for 16 h with control (DMSO), BAF (200 nM), RAP (20 nM), RAP + BAF, or PP242 (100 nM). (**d**) Top, western blot of GEMIN4 immunoprecipitates (IP) from HeLa cells. Bottom, western blot analysis of GEMIN4 in immunoprecipitates of anti-NDP52, -p62 or control antibody from HeLa cells. (**e**) Western blot of DICER immunoprecipitates from HeLa cells. (**f**) Western blot of AGO2 immunoprecipitates from HeLa cells. (**g**) Western blot analysis of GEMIN4, compared with loading controls (DCP1A, CLN3) in HeLa cells treated with control siRNA or siRNA targeting GEMIN3 and GEMIN4. (**h**) Western blot analysis of HeLa cells treated with indicated combinations of control siRNA or siRNA targeting GEMIN3, GEMIN4 and ATG5. Western blot analysis of CLN3 and DCP1A are used to demonstrate equal loading of wells. (**i**) Western blot analysis with anti-UB monoclonal antibody (mono- and polyubiquitylated proteins, FK2 clone) in Flag immunoprecipitates performed under stringent denaturing conditions. Flag–AGO2 was induced for 24 h with tetracycline in HEK293T cells with Tet-inducible Flag–AGO2 stably integrated that had been treated 24 h before with the indicated siRNAs. (**j**) Western blot analysis of HeLa cells treated with control siRNA or siRNA targeting ATG5 for 24 h. TUBA, α-tubulin loading control. (**k**) Top, RT–qPCR analysis of miR-16 or let-7a levels in AGO2 immunoprecipitates from DMSO- and BAF-treated HeLa cells. Error bars represent s.e.m. Bottom, a representative western blot of AGO2 immunoprecipitates used in one replicate of these experiments. Uncropped images of blots are shown in Supplementary Fig. S3.

fractions and XRN2 levels were unaffected by ATG7 siRNA treatments (Supplementary Fig. S1c–d). miRNA are also destabilized by trimming–tailing, which generates diagnostic ladder-like patterns on northern blots[6]; however, we did not observe such patterns (Fig. 4a). This suggests that in autophagy-deficient cells, miRNA levels decrease independently of known pathways of miRNA degradation. Others have demonstrated that impediments to AGO-loading cause a drop in miRNA levels[16,28–30]. As DICER and AGO both bind miRNA–miRNA* duplexes and promote their loading into AGO (refs 17,29–31), DICER and AGO2 degradation through autophagy may modulate loading of AGO2 and, consequently, miRNA levels. To test directly for effects on AGO loading, miRNA–miRNA* complexes were incubated with lysates of HeLa cells subjected to various treatments. In lysate from untreated cells, miRNA and miRNA* strands were detected in ultraviolet-crosslinked AGO2 complexes consistent with their loading into AGO2 (Supplementary Fig. S2). As expected, miRNA strands were more efficiently loaded into AGO2, retrieved by immunoprecipitation, than miRNA* strands (Fig. 4e–g and Supplementary Fig. S2a) and incorporation of both small RNA species was impeded by geldanamycin, an hsp90 inhibitor that blocks AGO loading with small RNAs (ref. 32) (Fig. 4e–g). Fewer miRNA and miRNA* strands were also loaded into AGO2 in lysates from BAF-treated cells (Fig. 4e–g), demonstrating that active autophagy is required for continued transfer of miRNA–miRNA* duplexes into AGO2. Consistent with a block in transfer of miRNA–miRNA* duplexes into AGO, the levels of miR16-1* and let-7a* were reduced proportionally to those of miR16-1 and let-7a when NDP52, ATG5 or ATG7 was depleted by siRNAs (Fig. 4d).

To determine the consequence of this defect in AGO-loading on miRNA activity while eliminating any potential impact of autophagy on pre-miRNA processing or upstream steps, we measured the activity of exogenously delivered siRNA–siRNA* duplexes. To also rule out any confounding, autophagy-unrelated effects of mTOR, such as generalized suppression of cap-dependent translation[33], the following experiments involved siRNAs targeting ATG5 or ATG7 to block autophagy at the level of autophagosome biogenesis, downstream of mTOR. In autophagy-deficient cells, a siRNA–siRNA* duplex, but not a missense control, silenced a *Renilla* reporter with partially complementary sites

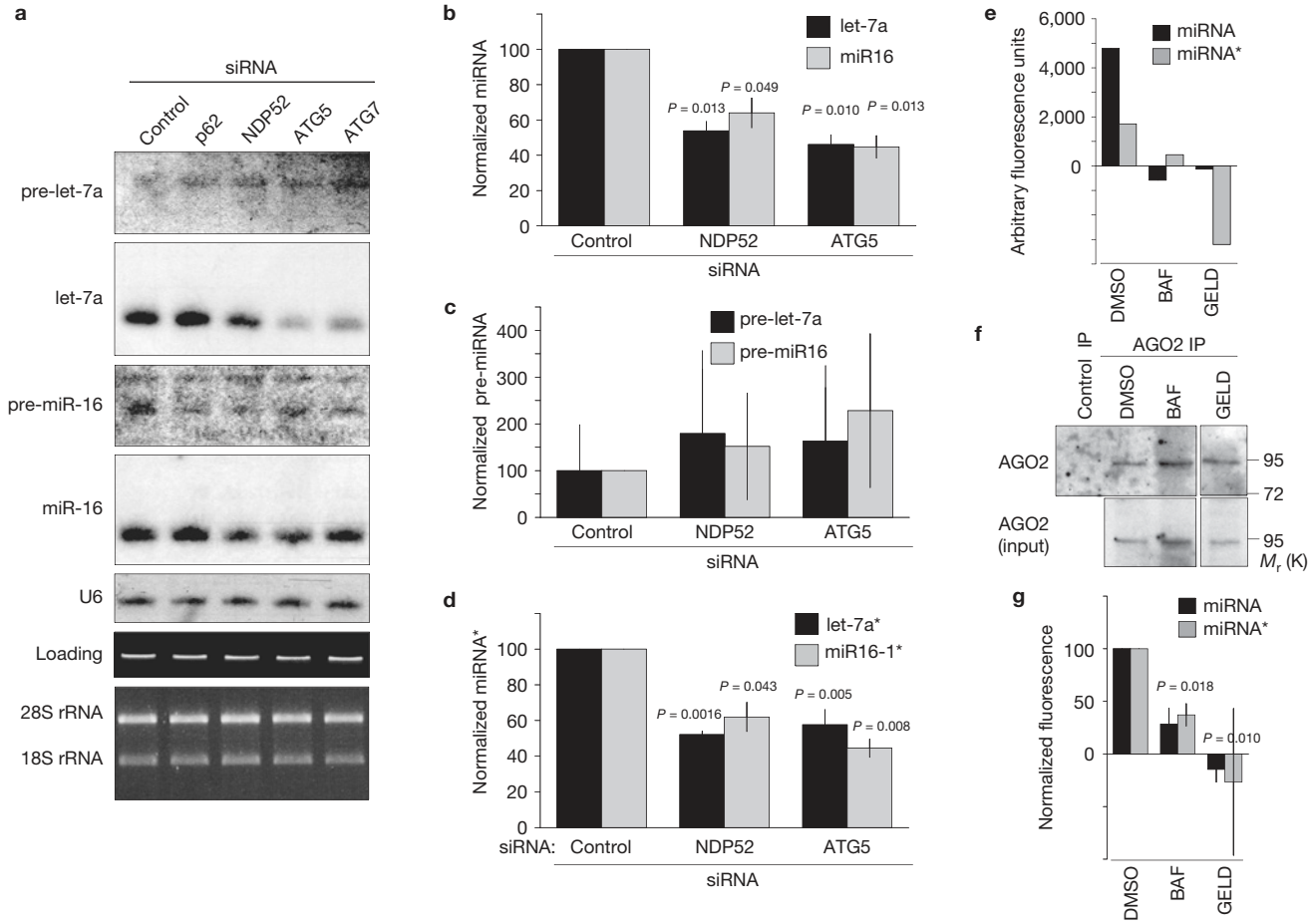

Figure 4 miRNA and miRNA* levels decrease when autophagy is inhibited for extended periods. (**a**) Northern blot of miR-16 and let-7a in HeLa cells treated with siRNA for 84 h. Levels of U6, ethidium-bromide-stained total RNA on northern membrane (loading) and 28S and 18S ribosomal RNA on 1% agarose gel are shown as controls for equal loading. (**b**–**d**) RT–qPCR analysis of let-7a and miR-16 (**b**), pre-let-7a and pre-miR-16 (**c**) and let-7a* and miR-16* (**d**) in HeLa cells depleted of NDP52 or ATG5 with siRNA (84 h). $n = 3$ independent experiments; error bars represent s.e.m. (**e**) Quantification of fluorescence signal in AGO2 immunoprecipitates from HeLa cell extracts incubated with duplexes of let-7a–let-7a* labelled on the 3′ end of either let-7 or let-7a* with FITC. Cells were treated 16 h before with DMSO (control), BAF (200 nm) or geldanamycin (10 μM). Representative results of one experiment are shown. (**f**) Western blot analysis of AGO2 immunoprecipitates (IP) used in **e**. (**g**) Normalized results of four independent experiments ($n = 4$) identical to **e**. Error bars represent s.e.m. Uncropped images of blots are shown in Supplementary Fig. S3.

less efficiently than in control cells (Fig. 5a). These data demonstrate that autophagy is required for continued loading of miRNA–miRNA* duplexes into AGO and for their durable activity (Figs 4e–g and 5a), consistent with homeostatic degradation of DICER–AGO2 complexes by autophagy (Figs 1 and 2). To determine whether autophagy also regulates endogenous miRNA action, we employed a second dual-luciferase reporter[34] (Fig. 5b, diagram) for let-7 activity, which was indeed less efficiently repressed on depletion of NDP52, ATG5 or ATG7 (Fig. 5b). Furthermore, accumulation of endogenous RAS (targeted by let-7; ref. 35), HMGA2 (targeted by let-7; ref. 36) or cyclin-dependent kinase 6 (CDK6, targeted by let-7a and miR-16; ref. 36) was increased in ATG7-depleted cells, reaching levels similar to those observed when miRNA activity was directly inhibited with antagomirs (Fig. 5c).

As *DICER* mRNA is a direct target of let-7a (ref. 9), we finally investigated the contribution of decreased let-7a activity (Fig. 5b,c) to the overall gain in DICER protein levels observed on autophagy inhibition. Confirming repression of the DICER 3′UTR by let-7a, a let-7 antagomir increased the stability of the DICER 3′UTR in a dual-luciferase assay (Fig. 5d) and caused endogenous DICER protein to over-accumulate (Fig. 5e). DICER protein also accumulated in cells depleted of ATG7, reaching levels higher than those attained with the let-7 antagomir alone (Fig. 5e), consistent with autophagy regulating DICER by both protein degradation (Figs 1 and 2) and miRNA-mediated post-transcriptional processes (Fig. 5d,e). Moreover, inhibition of autophagy with ATG5-targeting siRNAs also augmented translation controlled by the DICER 3′UTR (Fig. 5f). Together, these results suggest that autophagy regulates DICER at two distinct levels: through NDP52-dependent protein degradation (Figs 1 and 2) and through post-transcriptional control of the DICER transcript. Thus, autophagy engages DICER, and possibly AGO2, in multilayered regulatory mechanisms impacting miRNA accumulation and activity.

Previous evidence hinted that miRNA-free AGO2 is degraded by an unknown mechanism: obstructing DICER-dependent AGO2 loading with miRNA–miRNA* duplexes caused AGO2 degradation in a manner only partly rescued with the proteasome inhibitor MG132 (ref. 8). Similarly, plant Ago1 is degraded possibly in an unloaded form[37] in an MG132-independent but autophagy-dependent manner[38]. We have shown that the critical components of miRNA biogenesis complexes,

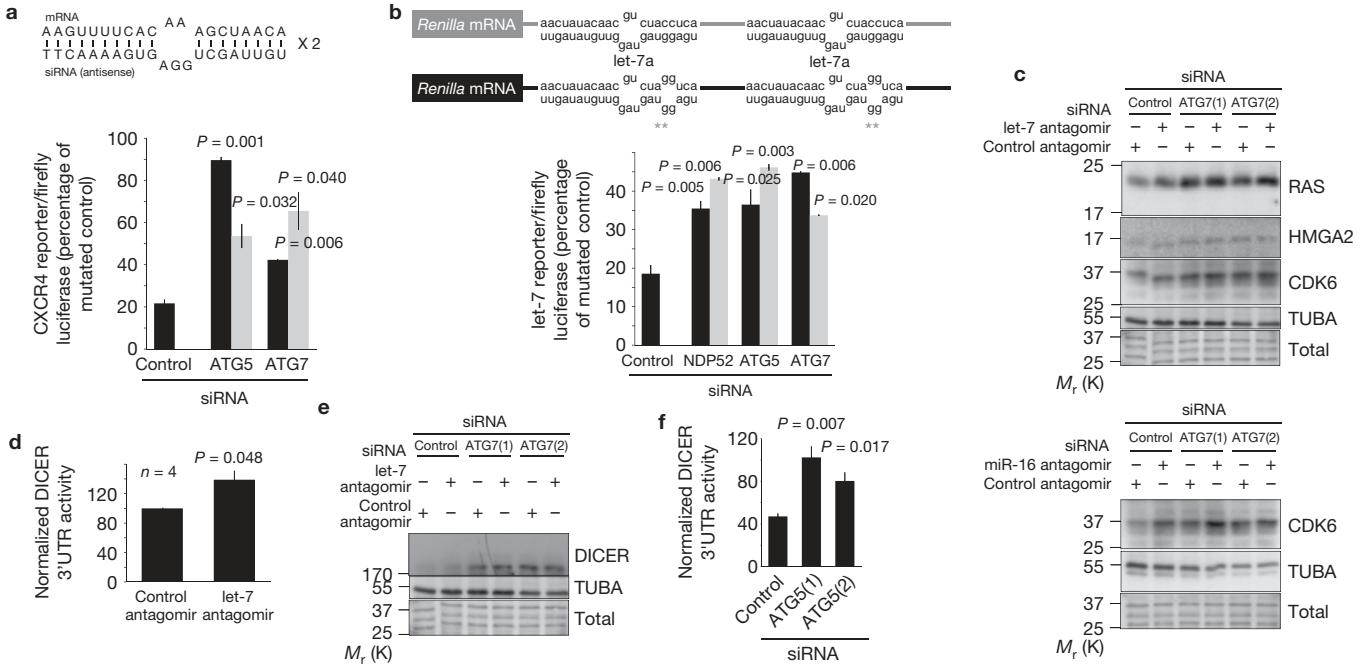

Figure 5 Autophagy is required for miRNA activity and engages post-transcriptional regulation of DICER. (**a**) *Renilla* luciferase expression controlled by an exogenous siRNA–siRNA* duplex targeting two partially complementary sites in HeLa cells depleted of ATG5 or ATG7 with siRNA (black and grey bars correspond to two independent siRNAs). Results are normalized to firefly luciferase and *Renilla* luciferase expression in cells treated with a nonspecific siRNA–siRNA* duplex. $n = 2$ independent experiments. (**b**) *Renilla* luciferase expression controlled by let-7 in HeLa cells depleted of NDP52 or ATG5 with siRNA (black and grey bars are independent siRNAs). Results are normalized to firefly luciferase and a version of the *Renilla* luciferase construct with mutated let-7 binding sites. $n = 3$ independent experiments. The asterisks denote mutations in the let-7 target sites of the reporter. (**c**) Western blot analysis of endogenous miRNA-repressed proteins (RAS, HMGA2 and CDK6 are repressed by let-7; CDK6 is also repressed by miR-16 (bottom panel)) or control (TUBA, α-tubulin) in HeLa cells treated with control siRNA or either of two independent siRNAs targeting ATG7. Cells were treated in parallel with nonspecific antagomir or let-7 targeting antagomir. (**d**) *Renilla* luciferase expression controlled by the DICER 3′UTR in HeLa cells treated with control antagomir or anti-let-7 antagomir. (**e**) Western blot analysis of DICER in HeLa cells treated with control siRNA or either of two independent siRNAs targeting ATG7. Cells were also treated with nonspecific antagomir or let-7 targeting antagomir. (**f**) *Renilla* luciferase expression controlled by the DICER 3′UTR in HeLa cells treated with either of two independent siRNAs targeting ATG5 or a control siRNA. All error bars are s.e.m. Uncropped images of blots are shown in Supplementary Fig. S3.

DICER and AGO2, are selectively degraded through NDP52-dependent autophagy while inactive, that is, without their pre-miRNA, miRNA or miRNA* cargoes. Removal by autophagy of these inactive DICER–AGO2 complexes from the cellular pool seems required for persistent function of the remaining DICER–AGO2 complexes in stabilizing miRNA–miRNA* duplexes and transferring them into AGO (refs 29,30). Indeed, autophagy-deficient cells exhibit decreased AGO-loading with miRNA and miRNA* (Fig. 4e,g), diminished miRNA and miRNA* levels (Fig. 4a–d) and reduced silencing activity of exogenous siRNA–siRNA* duplexes (Fig. 5a). Hence, inactive DICER–AGO2 complexes targeted to autophagy may compete with active complexes for cellular cofactors, substrates or targets. Strikingly, therefore, in both plants[38] and metazoans, autophagy may be required for homeostatic clearance of miRNA-free DICER and AGO pools.

NDP52 and p62 can recruit ubiquitylated and ubiquitin-independent cargoes for autophagic degradation[13,15]. Similarly, our evidence suggests that multiple recognition events might recruit DICER and AGO2 to NDP52-dependent autophagy, including GEMIN4 association and ubiquitylation. Provision of selectivity to autophagy is increasingly recognized to require complex and multiple recognition events that will certainly deserve careful attention in the future. Our findings predict that AGO-loading, miRNA abundance and miRNA activity may be perturbed by pathogens, stresses or diseases, known to alter autophagy[11]. Autophagy regulators, including *PIK3CA*, *ATG6* (beclin 1) and *PTEN*, are, for instance, frequently mutated in cancers and several core autophagy genes were identified as tumour suppressors[39]. Consistent with this idea, autophagy is often aberrantly inhibited in cancer cells[39]. Incidentally, several studies have also reported global downregulation of miRNAs in most types of tumour, correlating with less differentiated and proliferative states[40]. Our results thus suggest that autophagy inhibition in cancer cells may well be causal in this global decrease in miRNA levels, providing a potential mechanistic link between these two seemingly disparate phenomena. □

METHODS

Methods and any associated references are available in the online version of the paper.

Note: Supplementary Information is available in the online version of the paper

ACKNOWLEDGEMENTS

The authors would like to thank M. Johnston (ETH-Zurich, Switzerland) for providing HEK293T cells stably transfected with Tet-inducible Flag–AGO2 as well as the protocol for detection of ubiquitylated Flag–AGO2. Financial support was provided by a core grant from ETH-Z to O.V., and the Pasteur Institute to P.C. S.M. is a Wellcome Trust Research Career Development Fellow. The authors thank K. McGourty and D. Li for helpful discussions.

AUTHOR CONTRIBUTIONS

D.G. conceived the hypothesis. D.G., S.M., F.J. and Y.S. performed and analysed experiments. D.G., S.M. and O.V. designed the overall research. D.G., S.M., P.C. and O.V. wrote the manuscript.

COMPETING FINANCIAL INTERESTS

The authors declare no competing financial interests.

Published online at www.nature.com/doifinder/10.1038/ncb2611
Reprints and permissions information is available online at www.nature.com/reprints

1. Kim, V. N., Han, J. & Siomi, M. C. Biogenesis of small RNAs in animals. *Nat. Rev. Mol. Cell Biol.* **10,** 126–39 (2009).
2. Krol, J., Loedige, I. & Filipowicz, W. The widespread regulation of microRNA biogenesis, function and decay. *Nat. Rev. Gene.* **11,** 597–610 (2010).
3. Siomi, H. & Siomi, M. C. Post transcriptional regulation of microRNA biogenesis in animals. *Mol. Cell* **38,** 323–32 (2010).
4. Eulalio, A., Huntzinger, E. & Izaurralde, E. GW182 interaction with Argonaute is essential for miRNA-mediated translational repression and mRNA decay. *Nat. Struct. Mol. Biol.* **15,** 346–53 (2008).
5. Bazzini, A. A., Lee, M. T. & Giraldez, A. J. Ribosome profiling shows that miR-430 reduces translation before causing mRNA decay in zebrafish. *Science* **336,** 233–237 (2012).
6. Ameres, S. L. *et al.* Target RNA-directed trimming and tailing of small silencing RNAs. *Science* **328,** 1534–9 (2010).
7. Chatterjee, S. & Grosshans, H. Active turnover modulates mature microRNA activity in *Caenorhabditis elegans*. *Nature* **461,** 546–9 (2009).
8. Johnston, M., Geoffroy, M. C., Sobala, A., Hay, R. & Hutvagner, G. HSP90 protein stabilizes unloaded argonaute complexes and microscopic P-bodies in human cells. *Mol. Biol. Cell* **21,** 1462–9 (2010).
9. Mayr, C. & Bartel, D. P. Widespread shortening of 3′UTRs by alternative cleavage and polyadenylation activates oncogenes in cancer cells. *Cell* **138,** 673–84 (2009).
10. Vaucheret, H., Vazquez, F., Crete, P. & Bartel, D. P. The action of ARGONAUTE1 in the miRNA pathway and its regulation by the miRNA pathway are crucial for plant development. *Genes Dev.* **18,** 1187–97 (2004).
11. Mizushima, N. & Komatsu, M. Autophagy: renovation of cells and tissues. *Cell* **147,** 728–41 (2011).
12. Pankiv, S. *et al.* p62/SQSTM1 binds directly to Atg8/LC3 to facilitate degradation of ubiquitinated protein aggregates by autophagy. *J. Biol. Chem.* **282,** 24131–45 (2007).
13. Thurston, T. L., Wandel, M. P., von Muhlinen, N., Foeglein, A. & Randow, F. Galectin 8 targets damaged vesicles for autophagy to defend cells against bacterial invasion. *Nature* **482,** 414–8 (2012).
14. Shaid, S., Brandts, C. H., Serve, H. & Dikic, I. Ubiquitination and selective autophagy. *Cell Death Diff.* http://dx.doi.org/10.1038 (2012).
15. Watanabe, Y. & Tanaka, M. p62/SQSTM1 in autophagic clearance of a non-ubiquitylated substrate. *J. Cell Sci.* **124,** 2692–701 (2011).
16. Gibbings, D. J., Ciaudo, C., Erhardt, M. & Voinnet, O. Multivesicular bodies associate with components of miRNA effector complexes and modulate miRNA activity. *Nat. Cell Biol.* **11,** 1143–9 (2009).
17. Haase, A. D. *et al.* TRBP, a regulator of cellular PKR and HIV-1 virus expression, interacts with Dicer and functions in RNA silencing. *EMBO Rep.* **6,** 961–7 (2005).
18. Lee, Y. S. *et al.* Silencing by small RNAs is linked to endosomal trafficking. *Nat. Cell Biol.* **11,** 1150–6 (2009).
19. Gibbings, D. & Voinnet, O. Control of RNA silencing and localization by endolysosomes. *Trends Cell Biol.* **20,** 491–501 (2010).
20. Friend, K. *et al.* A conserved PUF-Ago-eEF1A complex attenuates translation elongation. *Nat. Struct. Mol. Biol.* **19,** 176–83 (2012).
21. Pare, J. M. *et al.* Hsp90 regulates the function of argonaute 2 and its recruitment to stress granules and P-bodies. *Mol. Biol. Cell* **20,** 3273–84 (2009).
22. Liu, J., Valencia-Sanchez, M. A., Hannon, G. J. & Parker, R. MicroRNA-dependent localization of targeted mRNAs to mammalian P-bodies. *Nat. Cell Biol.* **7,** 719–23 (2005).
23. Mizushima, N., Yoshimori, T. & Levine, B. Methods in mammalian autophagy research. *Cell* **140,** 313–26 (2010).
24. Marzella, L., Ahlberg, J. & Glaumann, H. Isolation of autophagic vacuoles from rat liver: morphological and biochemical characterization. *J. Cell Biol.* **93,** 144–54 (1982).
25. Di, Y. *et al.* HCC-associated protein HCAP1, a variant of GEMIN4, interacts with zinc-finger proteins. *J. Biochem.* **133,** 713–8 (2003).
26. Meister, G. *et al.* Identification of novel argonaute-associated proteins. *Curr. Biol.* **15,** 2149–55 (2005).
27. Mourelatos, Z. *et al.* miRNPs: a novel class of ribonucleoproteins containing numerous microRNAs. *Genes Dev.* **16,** 720–8 (2002).
28. Gantier, M. P. *et al.* Analysis of microRNA turnover in mammalian cells following Dicer1 ablation. *Nucleic Acids Res.* **39,** 5692–703 (2011).
29. Chendrimada, T. P. *et al.* TRBP recruits the Dicer complex to Ago2 for microRNA processing and gene silencing. *Nature* **436,** 740–4 (2005).
30. Sakurai, K. *et al.* A role for human Dicer in pre-RISC loading of siRNAs. *Nucleic Acids Res.* **39,** 1510–25 (2011).
31. Noland, C. L., Ma, E. & Doudna, J. A. siRNA repositioning for guide strand selection by human Dicer complexes. *Mol. Cell* **43,** 110–21 (2011).
32. Iwasaki, S. *et al.* Hsc70/Hsp90 chaperone machinery mediates ATP-dependent RISC loading of small RNA duplexes. *Mol. Cell* **39,** 292–9 (2010).
33. Mamane, Y., Petroulakis, E., LeBacquer, O. & Sonenberg, N. mTOR, translation initiation and cancer. *Oncogene* **25,** 6416–22 (2006).
34. Doench, J. G. & Sharp, P. A. Specificity of microRNA target selection in translational repression. *Genes Dev.* **18,** 504–11 (2004).
35. Slack, F. let-7 microRNA reduces tumor growth. *Cell Cycle* **8,** 1823 (2009).
36. Obad, S. *et al.* Silencing of microRNA families by seed-targeting tiny LNAs. *Nat. Genet.* **43,** 371–8 (2011).
37. Csorba, T., Lozsa, R., Hutvagner, G. & Burgyan, J. Polerovirus protein P0 prevents the assembly of small RNA-containing RISC complexes and leads to degradation of ARGONAUTE1. *Plant J. Cell Mol. Biol.* **62,** 463–72 (2010).
38. Derrien, B. *et al.* Degradation of the antiviral component ARGONAUTE1 by the autophagy pathway. *Proc. Natl Acad. Sci. USA* **109,** 15942–15946 (2012).
39. Wander, S. A., Hennessy, B. T. & Slingerland, J. M. Next-generation mTOR inhibitors in clinical oncology: how pathway complexity informs therapeutic strategy. *J. Clin. Inv.* **121,** 1231–41 (2011).
40. Lu, J. *et al.* MicroRNA expression profiles classify human cancers. *Nature* **435,** 834–8 (2005).

DOI: 10.1038/ncb2611

METHODS

Cells and transfections. HeLa (CCL-2), HEK293T (CRL-1573), MDA-231 (HTB-26), T47D (30-4500K) and MDA-435 (HTB-129) cells were obtained from the American Type Culture Collection and grown in DMEM supplemented with 10 mM HEPES and 10% FBS. Cells were transfected with siRNA using RNAiMax (Invitrogen). Plasmids were transfected with GeneJuice (Merck) or Lipofectamine 2000 (Invitrogen).

Antibodies and reagents. The following primary antibodies were used in this study: anti-human AGO1 (rat clone 4B8) and AGO2 (rat clone 11A9; ref. 41), serum 18033 recognizing TNRC6A-C (ref. 42; human, gift from M. Fritzler, University of Calgary, Canada), anti-DICER (mouse, clone 13D6, Abcam), anti-ALIX (mouse, clone 2H12, Abcam), anti-α-tubulin (mouse, clone DM1A, Sigma-Aldrich), anti-NDP52 (rabbit, ab68588, Abcam), anti-SQSTM1 (mouse, clone 3, BD Biosciences), anti-mono- and -poly-UB (clone FK2, MBL International), anti-GEMIN4 (clone 17D10, Millipore), anti-DCP1A (rabbit, gift from J. Lykke-Andersen, University of Colorado, USA), anti-CLN3 (ab75959, Abcam), anti-EEF1A1 (mouse, clone CBP-KK1, Millipore), anti-FXR1 (3FX, a gift from J. L. Mandel, IGBMC, Illkirch, France), anti-FITC (clone FITC-9, Ebioscience), anti-Ras (3965), anti-Cdk6 (3136) and anti-Hmga2 (5269, Cell Signaling Technology). All antibodies were used at dilutions of 1/1,000 for western blot except anti-DICER (10 μg ml^{-1}, western, confocal, electron microscopy) and anti-TUBA (1/20,000, western). For immunoprecipitations 3 μg of antibody was used.

Locked nucleic acid antagomirs (octamers) complementary to the seed sequences (nucleotides 2–8) of let-7 or miR-16 or a control antagomir were synthesized and used as described previously[36] (Exiqon). These consisted of: let-7 LNA antagomir 5′-ACTACCTC-3′, miR16 LNA antagomir 5′-GTGCTGCT-3′ and control LNA antagomir 5′-TCATACTA-3′. siRNA targeting the CXCR4 luciferase reporter and a control were synthesized (Sigma Proligo) as described previously[43].

RAP (20 nM, 24 h or 48 h; experiments with PP242) and BAF (200 nM, 16 h; ref. 44) were obtained from Merck. PP242 (100 nM, 48 h) and CQ (20 μM, 16 h) were obtained from Sigma-Aldrich and used at the doses and for the durations in brackets. Geldanamycin (Sigma-Aldrich) was used at 10 μM, 16 h). All were resuspended in cell-culture-grade dimethylsulphoxide (DMSO).

Silencer Select siRNAs (Ambion) were used in this study. Specifically, the siRNAs used were: ATG5 5′-AUAUCUCAUCCUGAUAUAGCgt-3′ (siRNA ID s18160) and 5′-AUGAGCUUCAAUUGCAUCCtt-3′ (siRNA ID s18158), ATG7 siRNA 5′-UGAACUCCAAUGUUAAGCGag-3′ (siRNA ID s20651) and 5′-UGGUGUUAUACAGUGUUCCaa-3′ (siRNA ID s20650), p62 5′-siRNAUUUAAUGUAGAUUCGGAAGat-3′ (siRNA ID s16962) and 5′-UCUUUUCCCUCCGUGCUCCac-3′ (siRNA ID s16960), NDP52 5′-siRNAAAAGUAACCCACAUGAAGGtg-3′ (siRNA ID s19996) and 5′-UUUGUUG-UUUAGGUCAAUGgg-3′ (siRNA ID s19994), GEMIN4 5′-siRNAUUCGGCAGA-AGUGUCAACGgt-3′ (siRNA ID s27064) and 5′-ACCUCUUCAACAUCUAACCtc-3′ (siRNA ID s27066) and GEMIN3 5′-siRNAUGCUAUACCAUAUGUAUGCac-3′ (siRNA ID s22143).

Cell lysates and immunoprecipitations. Cells were scraped in cell lysis buffer PBS, 1% (v/v) NP–40, 10% (v/v) glycerol and Roche Complete Protease Inhibitor without EDTA). Cells were lysed for 30 min (4 °C) and centrifuged (1,000*g*, 5 min).

Detection of ubiquitylated AGO2. HEK293T Flp-In cells stably expressing Tet-inducible Flag–AGO2 (ref. 8) were transfected with siRNA 24 h before the addition of 100 ng ml^{-1} tetracycline for a further 24 h. Cells were scraped in cold PBS, centrifuged (200 g, 5 min) and the pellet lysed with 220 μl of boiling stringent lysis buffer (25 mM HEPES at pH 7.5, 150 mM NaCl, 0.5 mM EDTA, 1% SDS, 1% NP-40, 10% glycerol, 100 mM iodoacetamide, 1 mM dithiothreitol and protease inhibitor cocktail and phosphatase inhibitor; PhosStop). Cell lysate was immediately heated at 95 °C (5 min) and centrifuged (12,000*g*, 15 min). Cell lysate was added to anti-Flag magnetic beads (clone M2, Sigma-Aldrich) pre-washed with stringent lysis buffer (lacking iodacetamide). After 2 h incubation, the beads were washed three times in stringent lysis buffer (lacking iodoacetamide) before western blot analysis.

Plasmids. GFP–AGO2 (11590; ref. 45), HcRed–LC3 (24991), the let-7 reporter (pRL–TK–let7 A, 11324) and its control (pRL–TK–let7 B, 11325), the CXCR4 reporter (pRL-TK CXCR4 2x, 11306), pIS1-DICER-long (21649) and pIS1-DICER-long-mut-let-7 (21651) were from Addgene.

Immunofluorescence and confocal microscopy. Immunofluorescence microscopy was performed as previously described[16], using a confocal microscope (Zeiss LSM510). Briefly, cells were washed three times with PBS, fixed in 4% paraformaldehyde (10 min), washed in PBS containing 20 mM NH_4Cl (10 min) and permeabilized with 0.2% Triton X-100 in PBS (10 min). The cells were incubated overnight with primary antibody (DICER 10 μg ml^{-1}).

Quantitative analysis of confocal microscopy. Analysis was performed as previously described[46]. Three-dimensional confocal stacks were acquired for each sample (0.2 μm slice increment, ×63 objective, identical fluorescence settings). All three-dimensional images were analysed using an identical protocol in Volocity Image Analysis software (PerkinElmer). A fixed threshold of fluorescence intensity was applied to all anti-DICER, anti-NDP52 or HcRed–LC3 images and objects to minimize background. A protocol was implemented within Volocity to identify punctae of NDP52 or LC3 on the basis of: volume of >0.2 μm^3 (commensurate with autophagosomes) and fluorescence intensity above standardized threshold. Punctae identified by the Volocity protocol were finally triaged to eliminate extracellular or nuclear punctae inconsistent with autophagosomes. The fluorescence intensities for all DICER proteins co-localized with punctae of NDP52 or LC3 were then summed across the entire microscope field, and several microscope fields were averaged within each treatment and experiment. Data from each experiment were expressed as the ratio of the total fluorescence signal of DICER co-localized with NDP52 or LC3 in drug-treated cells compared with control cells prepared in parallel. Ratios of co-localized fluorescence signal were then averaged across experiments (mean ± s.e.m.). At least 50 cells were quantified per experiment for each condition in a minimum of 4 independent experiments (>1,000 co localization events).

Costes' method[47], Fay's method or van Steensel's method embedded within the Co-localisation Test ImageJ Plugin was used to determine whether apparent co-localization of DICER with NDP52 or LC3 was non-random. The algorithm for Costes' method was set to derive 75 distinct randomized images from the NDP52 or LC3 input images (parameters: pixel size 0.18 μm, 590 nm wavelength, numerical aperture 1.4, point spread function for image randomization 3 pixels). The algorithm compares $(\langle , \rangle)$ the amount of co-localization of DICER with NDP52 or LC3 with the amount of co-localization of DICER with each of the 75 randomly generated images. In none of the 75 randomly generated images for each condition did DICER co-localize with NDP52 or LC3 (controls, RAP or BAF) more than in physiological input images (0/75 in each condition). The probability was derived with a Chi-squared test (observed = 0/74, expected 37/37). Default settings were used for Fay's and van Steensel's tests. In Fay's method, no more than 2/41 randomized images exhibited more co-localization with DICER than the input image (Chi-squared test, $P < 0.0001$, observed 2/39, expected 21/20). In van Steensel's method, no more than 2/75 randomized images exhibited more co-localization with DICER than the input image (Chi-squared test, $P < 0.0001$, observed 2/73, expected 37/38).

Electron microscopy. Electron microscopy was performed as described previously[48]. Briefly, cells were subjected to high-pressure freezing (Leica EMPACT2) and freeze substituted as follows: 72 h at −90 °C in 0.1% (v/v) uranyl acetate in anhydrous acetone, 1 °C h^{-1} increase in temperature up to −50 °C, 12 h incubation, rinses with acetone, rinses with ethanol, infiltration in lowicryl HM20, ultraviolet-light polymerization at −50 °C for 48 h and ultraviolet-light polymerization for 48 h at room temperature. After removal of the carrier, the samples were cut (Leica UCT) in 70 nm sections and collected on carbon/formvar-coated grids. Immunogold staining was perfomed in PHEM buffer (PIPES, HEPES, EGTA, $MgCl_2$). Samples were blocked (15 min blocking, 1% (v/v) bovine serum albumin, 0.1% (v/v) fish-skin gelatin) then incubated in primary antibodies (1 h, anti-Dicer clone 13D6 20 μg ml^{-1}), rinsed and incubated with goat anti-mouse (10 nm, Jackson Immunoresearch). After rinsing, the samples were post-fixed with 1% (v/v) glutaraldehyde and observed in a CM12 transmission electron microscope (Philips-FEI) at 80 kV. Images were acquired with an Orius 1000 CCD (charge-coupled device) camera (Gatan).

Density-gradient enrichment of autophagosomes. The protocol was adapted from ref. 24 according to ref. 49, with the exception that the cells were lysed in a Potter–Elvehjem homogenizer.

***In vitro* loading of miRNA and miRNA* into AGO2.** HeLa cells were disrupted according to the protocol for autophagosome fractionation. Extracts were centrifuged at 2,000*g* (5 min) and incubated with an RNA mimic of let-7a–let-7a* duplexes labelled on the 3′ end of either let-7a or let-7a* with FITC (Proligo, Sigma-Aldrich). Extracts were incubated at 37 °C for 1 h with intermittent mixing. Extracts were ultraviolet crosslinked (400 mJ cm^{-2}, mixed, 200 mJ cm^{-1}; ref. 2) as described previously[50]. AGO2 was immunoprecipitated and eluted as described previously[41]. Fluorescence quantification (BMG Polarstar Omega, 490 nm ± 10 nm excitation, 520 nm ± 10 nm emission) from control immunoprecipitations was subtracted to calculate the fluorescence intensity of AGO2-associated let-7a or let-7a*.

RT–qPCR. Total cellular RNA was extracted with Trizol. Eluates of immunoprecipitates were extracted with Trizol LS. RNA was treated with 1.2 µl DNAse (Promega) and 0.1 µl RNAseOut (Invitrogen) before RT–qPCR (miScript PCR system, Qiagen) with a Light Cycler 480 II (Roche).

The following primers were used: β-actin 5′-GGCATGGGTCAGAAGGATT-3′ and 5′-GGGGTGTTGAAGGTCTCAAA-3′, RRM2 5′-GACATCACTCCCATCCTCTGA-3′ and 5′-CCTTGCCTGTGAAGCTCATT-3′, DICER 5′-TGTTCCAGGAAGACCAGGTT-3′ and 5′-ACTATCCCTCAAACACTCTGGAA-3′, AGO1 5′-AAGAACATTTACACTGTCACAGCAC-3′ and 5′-TTGATGGAGACCTTAAAGATTCG-3′, AGO2 5′-CGGCAGGAAGAATCTATACACA-3′ and 5′-CGATCCTTGCCTTCTCCTG-3′, let-7a 5′-CCGGCGTGAGGTAGTAGGTTGT-3′, let-7a* 5′-CCGGCGCTATACAATCTACTG-3′, miR-16 5′-CCGGCGTAGCAGCACGTAAATA-3′, miR-16* 5′-CCGGCGCCAGTATTAACTGTGC-3′, RNU6B (control for miRNA and miRNA*) 5′-CCGGCGCGCAAGGATGACACGCAAATTCGTGAAGCGTTCCAT-3′, pre-miR-16 5′-GCAGCACGTAAATATTGGCGT-3′ and 5′-CAGCAGCACAGTTAAATACTGGAG-3′, pre-let-7d 5′-AACGCTTCACGAATTTGCGT-3′ and 5′-AAGGCAGCAGGTCGTATAGT-3′, and U6 (control for pre–miRNA) 5′-CTCGCTTCGGCAGCACA-3′ and 5′-AACGCTTCACGAATTTGCGT-3′.

Statistics. A paired *t*-test was used to examine the statistical significance of differences.

Analysis of miRNA association with AGO2. AGO2 was immunoprecipitated with 3 µg anti-AGO2 (clone 11A9) or control rat IgG2b. After washes, protein G beads were eluted with 50 µl 0.1 M glycine at pH 2.4 for 5 min on a shaker and 7 µl 1 M Tris–HCl at pH 8 was added to neutralize the elution buffer. The background level of miRNA detected in control immunoprecipitations was subtracted.

41. Rudel, S., Flatley, A., Weinmann, L., Kremmer, E. & Meister, G. A multifunctional human Argonaute2-specific monoclonal antibody. *RNA* **14,** 1244–53 (2008).
42. Eystathioy, T. *et al.* A phosphorylated cytoplasmic autoantigen, GW182, associates with a unique population of human mRNAs within novel cytoplasmic speckles. *Mol. Biol. Cell* **13,** 1338–51 (2002).
43. Doench, J. G., Petersen, C. P. & Sharp, P. A. siRNAs can function as miRNAs. *Gen. Dev.* **17,** 438–42 (2003).
44. Klionsky, D. J., Elazar, Z., Seglen, P. O. & Rubinsztein, D. C. Does bafilomycin A1 block the fusion of autophagosomes with lysosomes? *Autophagy* **4,** 849–950 (2008).
45. Jakymiw, A. *et al.* Disruption of GW bodies impairs mammalian RNA interference. *Nat. Cell Biol.* **7,** 1267–74 (2005).
46. Mesquita, F. S. *et al.* The Salmonella deubiquitinase SseL inhibits selective autophagy of cytosolic aggregates. *PLoS Pathog.* **8,** e1002743 (2012).
47. Costes, S. V. *et al.* Automatic and quantitative measurement of protein-protein colocalization in live cells. *Biophys. J.* **86,** 3993–4003 (2004).
48. Spiegelhalter, C. *et al.* From dynamic live cell imaging to 3D ultrastructure: novel integrated methods for high pressure freezing and correlative light-electron microscopy. *PLoS ONE* **5,** e9014 (2010).
49. Sahu, R. *et al.* Microautophagy of cytosolic proteins by late endosomes. *Dev. Cell.* **20,** 131–9 (2011).
50. Chi, S. W., Zang, J. B., Mele, A. & Darnell, R. B. Argonaute HITS-CLIP decodes microRNA-mRNA interaction maps. *Nature* **460,** 479–86 (2009).

nature cell biology

DOI: 10.1038/ncb2611

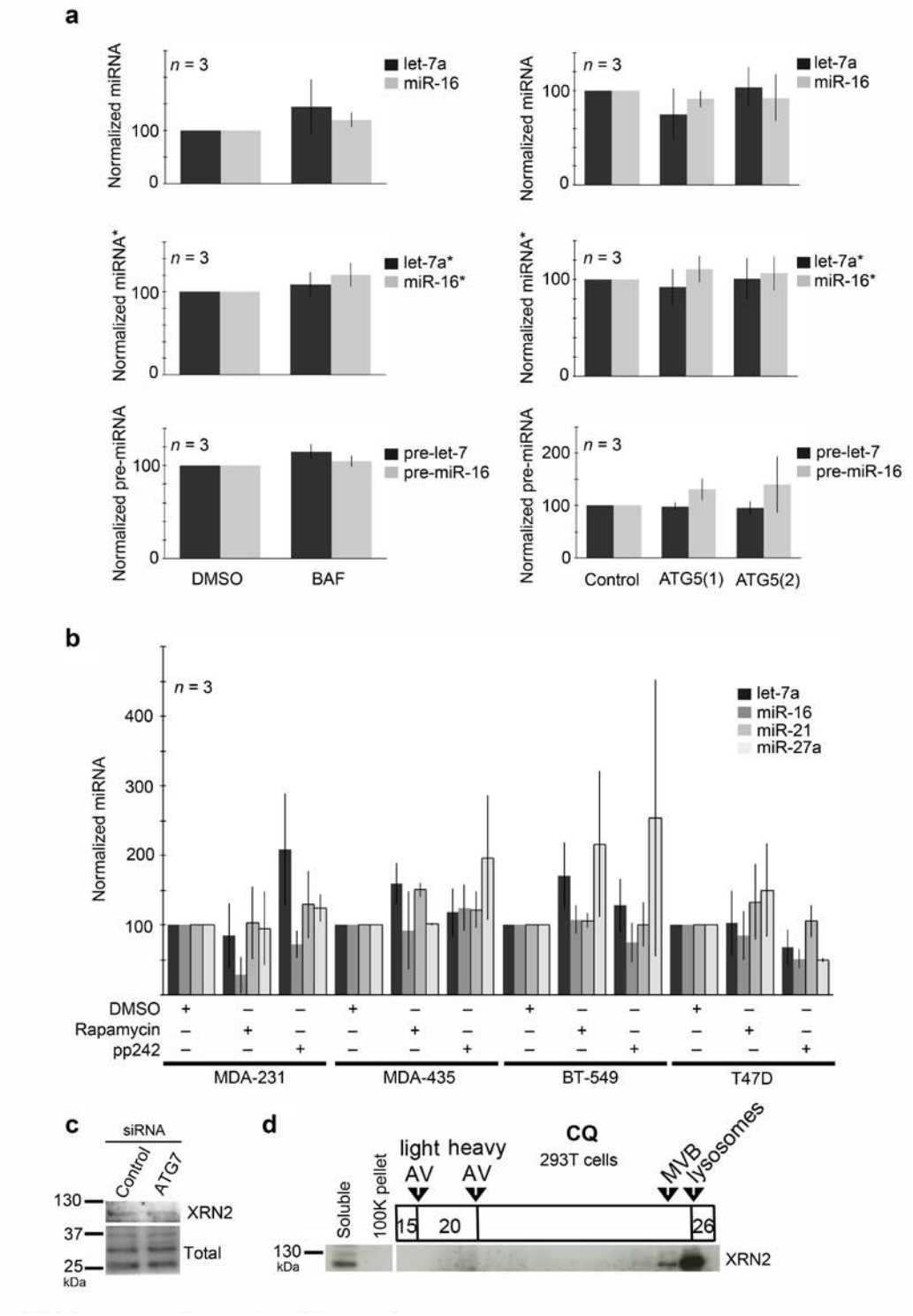

Figure S1 Short-term modulation of autophagy does not affect miRNA levels and XRN2 is not regulated by autophagy. (**a**) RT-qPCR analysis of levels of miRNA (miR-16, let-7a), and the corresponding miRNA* or pre-miRNA in HeLa cells treated with DMSO (control) or BAF for 12 h. ATG5(1) and ATG5(2) represent results with two independent siRNA. (**b**) RT-qPCR analysis of MDA-231, T47D and MDA-435 cells treated with DMSO, or inhibitors of mTORC1 (rapamycin) or mTORC1/2 (pp242) for 48 h. Error bars represent SEM. (**c**) Western blot of XRN2 in cells treated with siRNA targeting ATG7 or a control siRNA. Total protein stained by Coomassie blue serve as a loading control. (**d**) Western blot analysis of XRN2 in fractions from a discontinuous gradient of Histodenz™ (15%, 20%, 24%, 26%) described to enrich autophagosomes (light AV) and autophagolysosomes (heavy AV). 293T cells were treated with CQ (20 μM, 16 h). Fractions enriched in MVB and lysosomal markers are indicated. Material that was pelleted by centrifugation at 100,000 g (100K pellet) or that remained in solution after the 100,000 g spin (soluble) was not added to the gradient.

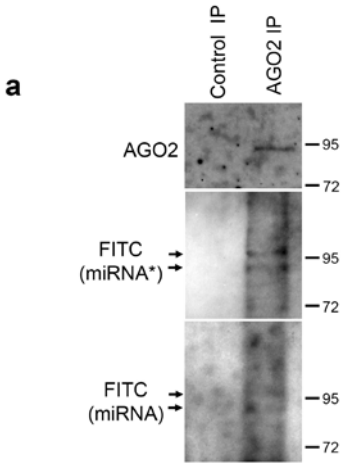

Figure S2 MiRNA and miRNA* added to *in vitro* AGO2-loading assay associate with AGO2. In HeLa cell extracts, following UV-cross-linking and AGO2 immunoprecipitation a fraction of AGO2 eluate was analyzed by western blot with anti-FITC mAb (to detect miRNA or miRNA* labeled 3' with FITC) and anti-AGO2 mAb. Anti-FITC mAb detected bands at masses coinciding with AGO2. Higher band may represent the mass-shift caused by covalent binding of AGO2 to RNA after UV-cross-linking. Similar mass shifts of AGO bound to single-stranded versus double-stranded RNA (miRNA + miRNA* or miRNA + mRNA target) have been described previously[50].